Current Science
CS 5 (5), 4440-4454 (2025)
Received 11 June 2025 | **Revised 13 July** 2025 | **Accepted 15 August** 2025 | **Online Available 15 September** 2025
https://doi.org/10.52845/CS/2025-5-5-10

Current Science

Current Science

OPEN ACCESS

ISSN(O)2795-8639

Original Article

Transition Investigation on Stress-Strain Relationship of Sand-Silt Mixtures from Check Dam Deposit in Loess Plateau

Ya Wang[1], Hongyu Wang[2,*], Liucheng Chang[3]

[1]School of Civil and Hydraulic Engineering, Ningxia University, Yinchuan, 750000, Ningxia, China; School of Information Engineering, Yinchuan University of Science and Technology, Yinchuan, 750000, Ningxia, China

[2]School of Civil and Hydraulic Engineering, Ningxia University, Yinchuan, 750000, Ningxia, China

[3]School of Civil and Hydraulic Engineering, Ningxia University, Yinchuan, 750000, Ningxia, China

[*]Corresponding Author: Hongyu Wang

Abstract:

To examine the influence of initial moisture content and confining pressure on the stress-strain characteristics of sand-silt mixtures (SSM), a series of consolidated drained triaxial shear tests were performed on reconstructed sand-silt mixtures with varying moisture contents (10%, 12%, 14%, and 16%). The results indicated that the stress-strain behavior of SSM is predominantly governed by the applied confining pressure, showing significant strain softening under low confining pressures and pronounced strain hardening under high confining pressures. Based on these experimental observations, a modified constitutive model, referred to as the Combined Plasticity Model (CPM), was developed by integrating elements of both the classical hardening model and the softening model. Moreover, a post-failure modulus was incorporated to describe the transition phenomena, and its transformation mechanism was thoroughly analyzed. Additionally, three illustrative case studies were provided to validate the analytical results and demonstrate their applicability through comparison with experimental data.

Keywords: Transition pattern; Stress-strain constitutive relationship; CPM model; Post-failure modulus

1. Introduction

Check dams are widely acknowledged as one of the most critical engineering measures for controlling soil erosion on the Loess Plateau. They play a pivotal role in sediment retention, floodwater detention and storage, improvement of arable land, and enhancement of productive conditions and ecological environments in loess regions [1-2]. However, due to relatively low initial design standards and insufficient maintenance practices, substantial sediment accumulation occurs within the reservoir areas [3], leading to various hazards. Consequently, reinforcement is essential to ensure their continued functionality. The technique of constructing siltation surface dams upstream of the main structure is extensively utilized for reinforcing check dams (see Fig. 1). Regarding the foundation, the mechanical properties of sediments are crucial for the stability of newly constructed dams built on the deposited alluvium in front of the dam. Numerous studies indicate that sediment layers are characterized by varying sand content, high water content, high water sensitivity, and compressibility [4-7]. These properties differ with depth, resulting in significant variations in soil behavior. Therefore, it is imperative to investigate how these variables influence the engineering properties of the deposited sediments.

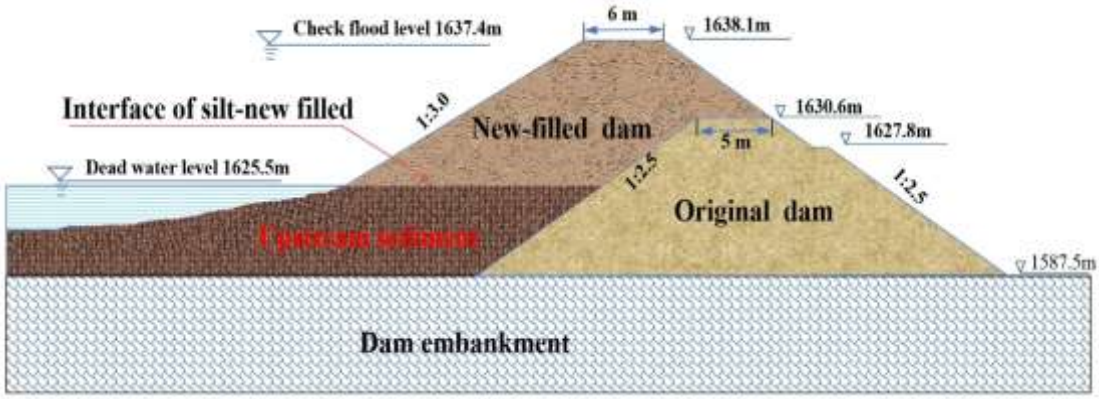

Fig.1 Upstream sediment heightening fill method diagram (Revised from [7])

Previous studies on dam decomposition predominantly focus on the influence of varying sand content on mechanical properties [8,9], compressive response [10], and liquefaction resistance [11]. However, limited attention has been given to the impact of moisture content on stress-strain behavior, which is a critical factor in understanding the strength characteristics of sand-silt mixtures. In the literature, numerous advanced soil models have been developed based on elastoplastic and mathematical theories. For strain hardening, model descriptions include exponential functions [12], nonlinear models such as the Duncan-Chang hyperbolic model [13], composite exponential-hyperbolic model [14], composite power-exponential model [15], composite tangent-exponential model [16], and power functions derived from fractional calculus theory [17]. Regarding strain softening, the full stress-strain curve is typically represented by the hump curve proposed by the Nanjing Hydraulic Research Institute (NHRI) [18] and nonlinear models based on exponential decay laws [19]. Undoubtedly, these models are theoretically robust; however, they often require parameters that are challenging to measure [20]. Specifically, in scenarios where the stress path is not overly complex or when there is insufficient data for an exploratory investigation into soil properties, simpler models such as the Duncan-Chang model and the hump curve are favored due to their minimal parameter requirements, clear physical meaning, and straightforward formulas [21]. In principle, the stress-strain relationship transitions from strain softening to strain hardening when external conditions vary, rather than remaining invariant. This phenomenon can be identified by analyzing stress-strain curves for materials such as Dashihe tailing sand with varying porosity [22], undisturbed loess under different confining pressures [23], Hangzhou soft clay under various pre-consolidation pressures [24], reconstituted calcareous sand samples at different initial densities and confining stresses [25], and clinker ash with diverse particle sizes and shapes [26]. While precise transition points may exist, specific pattern transition models are rarely provided in the literature. Consequently, employing either a strain softening model or a strain hardening model alone is insufficient to fully describe the stress-strain transition relationship. Instead, it is essential to adopt a unified stress-strain model that captures both behaviors comprehensively.

The aim and objective of this study are to investigate the strength behavior of sediment deposition upstream of a check dam under varying moisture contents using conventional triaxial tests. Based on the experimental results, a modified constitutive model incorporating a transition factor and post-failure modulus was developed to accurately capture both hardening and softening behaviors. The validity of the modified model and the transition prediction method was verified through three practical case studies. Furthermore, a comprehensive analysis of the underlying transition mechanism is presented.

2. Test Scheme

2.1 Materials and Methods

The remolded test samples were collected from the Zhu JiaGou check dam at depth of 0.5m to 2m in southern NingXia, China, as depicted in Fig.2. The basic physical property indexes of the tested sample are summarized in Table 1 and Fig. 3. Based on ASTM D2487-11 [27], the soil was

classified as a sand-silt mixture (SSM). Cylindrical samples with a diameter of 50 mm and a height of 100 mm were prepared indoors for testing purposes. Conventional consolidated drained triaxial tests were conducted on saturated samples under various moisture contents (10%, 12%, 14%, and 16%) and confining pressures (50 kPa, 100 kPa, 150 kPa, and 200 kPa). The test apparatus used in this study is an automatic stress-strain path triaxial apparatus (GSY-SYL-100), as illustrated in Fig.4, with a controlled shear rate of 0.005 mm/s.

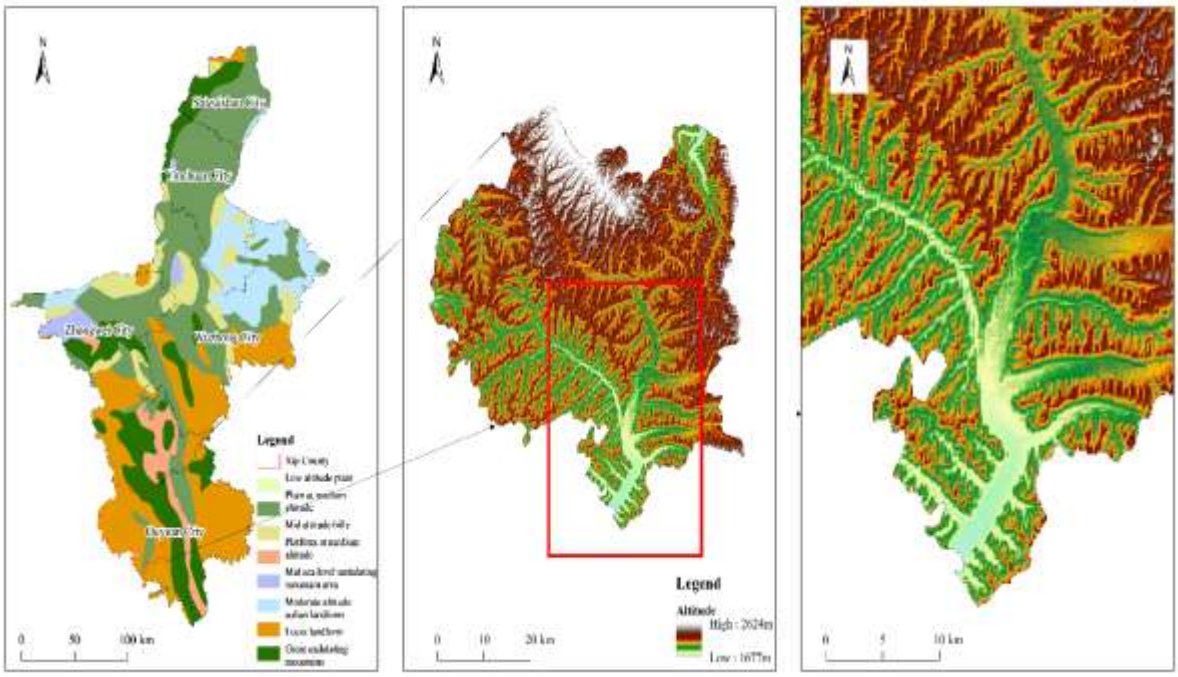

Fig. 2 Location of loess site and loess for test

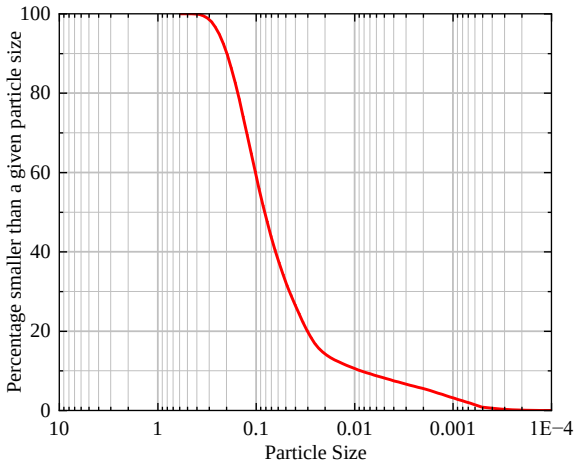

Fig. 3 Particle size distribution curve of SSM

Table 1 The basic physical indexes of tested SSM samples

Initial void ratio e_0	Specific gravity G_s	Dry density $\rho_d/\mathrm{g}\cdot cm^{-3}$	Optional water content $W_{op}/\%$	Liquid Limit $W_L/\%$	Plastic limit $W_P/\%$	Plasticity index I_P
2.05	2.67	1.66	14.8%	20.3	16.7	3.6

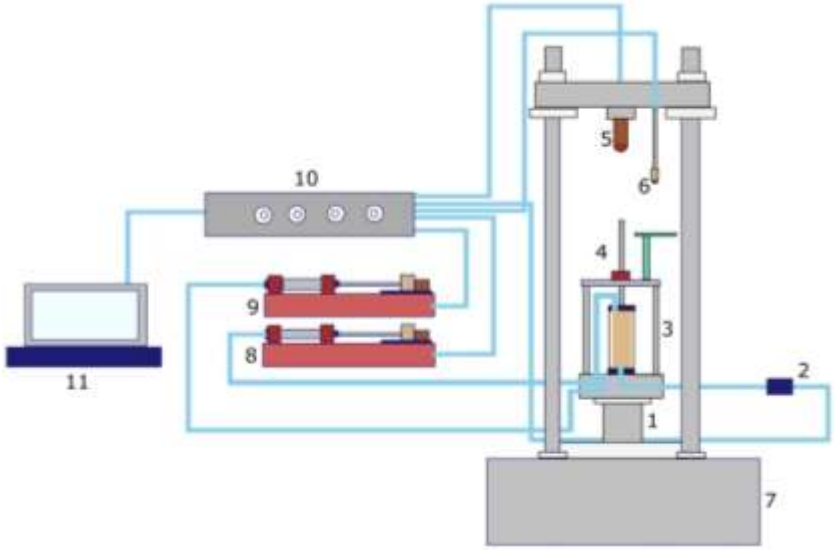

Fig. 4 The schematic diagram of stress-strain triaxial apparatus (GSY-SYL-100) 1 - Lifting table; 2 - Pore pressure sensor; 3 - Pressure gauge; 4 - Piston ejector rod; 5 - Pressure sensor; 6 - Displacement meter; 7 - Testing machine; 8 - Osmotic actuator; 9 - Confining pressure actuator; 10 - Data acquisition box; 11- Computer

The soil samples were subjected to a series of Consolidated Drained (CD) triaxial tests, conducted in three distinct phases: (1) The degree of saturation was enhanced to exceed 95% using the vacuum saturation method. (2) Fully saturated conditions were established by applying cycles of cell pressure and backpressure, ensuring a B-value of at least 0.98 prior to conducting the triaxial tests. (3) Drained shearing was performed on the soil specimens at a constant strain rate of 0.005 mm/s. During the shearing phase, four soil samples with varying moisture contents were tested until an axial strain of 25% was achieved. Each test was replicated twice to ensure result consistency and repeatability.

2.2 Stress-Strain Response

The stress-strain curves of SSM samples with a dry density of $\rho_d = 1.66\mathrm{g}\cdot cm^{-3}$ under varying water content are presented in Fig. 5. By analyzing the curve characteristics depicted in the figures, it is observed that the stress-strain curves under confining pressures of 50 kPa and 100 kPa, corresponding to soil moisture contents of 10%, 12%, and 14%, exhibit stress softening behavior at this specific dry density. Beyond the peak point of the curve, stress decreases as strain increases and asymptotically approaches a certain value. However, both the form and magnitude of the softening are influenced by the level of confining pressure. Lower confining pressures result in more pronounced stress softening with larger amplitudes, whereas higher confining pressures lead to reduced amplitude and a delayed onset of the softening stage. In contrast, for soil samples with a moisture content of 16%, the corresponding stress-strain curve demonstrates stress hardening behavior, where stress increases with strain and tends toward linearity. Notably, this phenomenon is more pronounced under higher confining pressures.

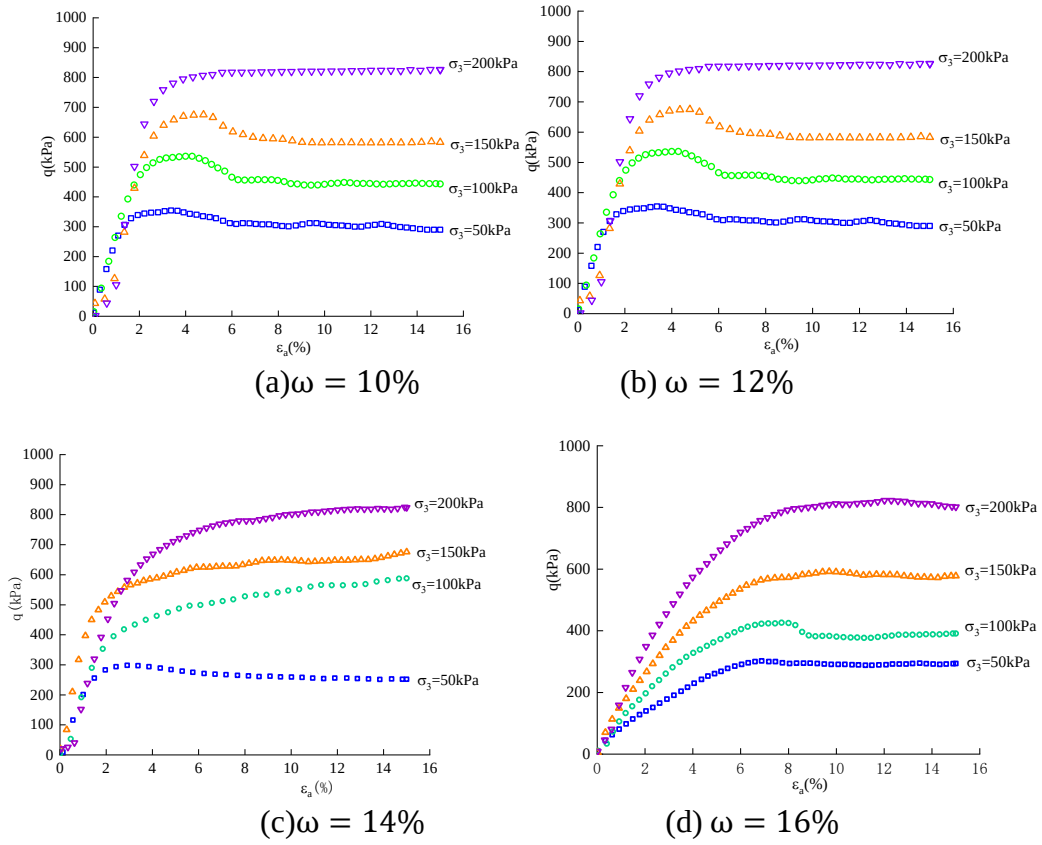

Fig.5 The stress-strain curves of are SSM under different water content

Moreover, it is evident from the analysis of stress variation characteristics depicted in Fig. 5 that for stress-strain curves with a peak point, an increase in confining pressure corresponds to a proportional rise in failure deviatoric stress. In cases where no peak exists on the stress-strain curve, higher confining pressures result in elevated deviatoric stresses at identical strain levels. This behavior can be attributed to the enhanced resistance to deformation exhibited by particle structures under increased confinement, which significantly influences both the strength and deformability properties of soils. Consequently, it is clear that confining pressure serves as a critical determinant factor influencing various mechanical properties of soils.

2.3 Peak Deviator Stress

The influence of water content on the magnitude of partial stress suggests that, under the sepcific confining pressure, the strength of the material follows a consistent variation trend (see Fig. 6). As water content increases, the peak strength progressively decreases. Specifically, the failure deviator stress at a water content of w = 10% is approximately 1.2 to 1.5 times higher than the maximum partial stress observed at a water content of w = 16%. This phenomenon demonstrates that the saturation of soil samples typically results in a substantial reduction in strength and a decline in the initial tangential modulus. In the context of SSM, a reduction in moisture content correlates with an increase in peak deviator stress, reflecting an inverse relationship between these two parameters. To precisely describe this relationship, a power function (Eq. 1) can be employed.

$$q_f = mw^n \#(1)$$

where m and n are the dimensionless parameters that are independent of the confining pressures. By fitting the curve, the dimensionless parameter varies significantly and can be written as follows:

$$m = -0.648{\sigma_3}^2 + 172\sigma_3 - 5940 \#(2a)$$

$$n = 9E - 5{\sigma_3}^2 - 0.023\sigma_3 + 0.515 \#(2b)$$

Combined with Eq.1-2, the relationship between peak deviatoric stress and moisture content with confining pressure can be obtained.

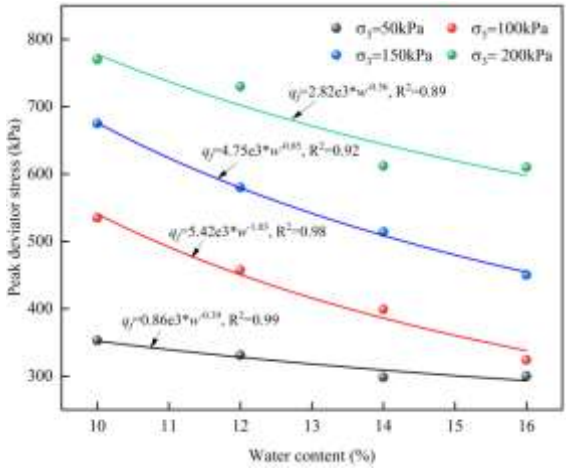

Fig. 6 The relationship between peak deviator stress and moisture content

3. Model Benchmark

3.1 Description of CPM Model

The strain hardening phenomenon can typically be simulated using the Duncan-Chang model (Pattern I), while the NHRI model (Pattern II) is also capable of simulating this phenomenon. However, it has been observed that Pattern I adequately describes the strain hardening curve of SSM but fails to accurately capture its strain softening behavior. Conversely, although Pattern II effectively characterizes the strain softening curve of SSM under confining pressures less than 150 kPa, it does not sufficiently represent the strain hardening curve when fitting experimental data. To address these limitations and account for both strain transitions as well as practical applicability in modeling both hardening and softening curves, a new composited model (CPM), referred to hereafter as Pattern III, is proposed by integrating features of Pattern I and Pattern II. This novel model facilitates further investigation into parameter relationships.

$$q = \sigma_1 - \sigma_3 = \frac{\varepsilon_a}{a + b\varepsilon_a + \mathrm{g}\sqrt{\varepsilon_a}} \#(3)$$

Where q is stress difference; ε_a *and* $(\sigma_1 - \sigma_3)$ denote the axial strain and deviatoric stress respectively; *a*, *b* and *c* are fitting parameters. g denotes the transition factor.

By differentiating Eq. (1), the following equation can be obtained:

$$\frac{d(\sigma_1 - \sigma_3)}{d\varepsilon_1} = \frac{c\varepsilon_1 + 2a\sqrt{\varepsilon_1}}{2\sqrt{\varepsilon_1}(a + c\varepsilon_1 + c\sqrt{\varepsilon_1})^2} \#(4)$$

$\frac{d(\sigma_1-\sigma_3)}{d\varepsilon_1}$ is an increasing function when $\varepsilon_1 < \frac{4a^2}{c^2}$; while $\frac{d(\sigma_1-\sigma_3)}{d\varepsilon_1}$ is a decreasing function when $\varepsilon_1 > \frac{4a^2}{c^2}$. Hence, strain-softening behavior can be characterized using Eq. (3). When c=0, Eq. (3) is the mathematical expression of the Duncan-Chang model used to approximate the strain-hardening stress-strain curves.

3.1.1 Parameter g

In Eq. (1), the transformation factor g represents a function of the confining pressure σ_3, which can be defined by Eq. (3).

$$\mathrm{g} = f(\sigma_3) = c(1 - < L >) \#(5)$$

$$L = \frac{|\sigma_3 - \sigma_{3,cr}|}{\sigma_3} \#(6)$$

In which L is initial state index related to confining pressure; $< L >$ is jump function, if $L > 0, < L >= 1,$; whereas $\mathrm{L} < 0, < L >= 0$; In particular, $\mathrm{g} = 0$, Eq. (1) can be further deduced to Duncan-Chang model.

3.1.2 Parameters a, b and c

For convenience, the model parameters *a*, *b* and *c* are expressed as follows (see Fig.7):

For strain hardening curve (Pattern I):

$$\begin{cases} a = \dfrac{1}{E_0} \\ b = \dfrac{1}{q_{ult}} \end{cases} \#\# \#(7)$$

For strain softening curve (Pattern II):

$$\begin{cases} a = \dfrac{1}{E_0} \\ b = \dfrac{1}{q_r} \\ c = \pm \dfrac{2}{E_0 \sqrt{\varepsilon_{af}}} \end{cases} \#(8)$$

Where E_0 is the initial tangent modulus; q_{ult} and q_r are the peak deviatoric stress and residual stress, respectively; ε_{af} is peak strain corresponding to peak stress.

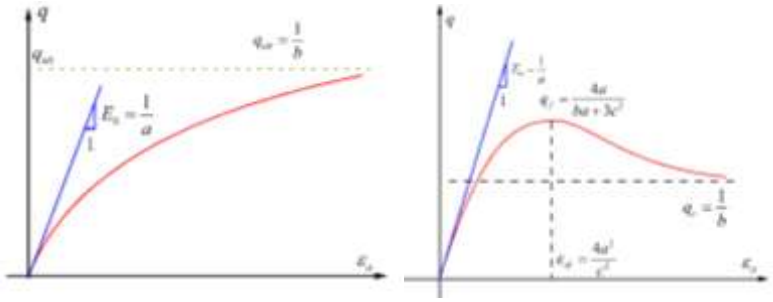

(a)strain hardening (b)strain softening

Fig.7 The physical meaning of model Parameters

3.2 Post-Failure Modulus

To conduct a comprehensive analysis of the stress-strain curve transition in SSM, this study adopts the concept of post-failure modulus E_{post}. As illustrated in Fig. 9 and defined below, E_{post} is formally introduced as follows [28]:

$$E_{post} = \frac{q_{post} - q_f}{\varepsilon_{post} - \varepsilon_f} \#(9)$$

where ε_f and q_f denote the failure strain and corresponding strength; ε_{post} and q_{post} denote the strain and corresponding strength after damage, as displayed in Fig. 8.

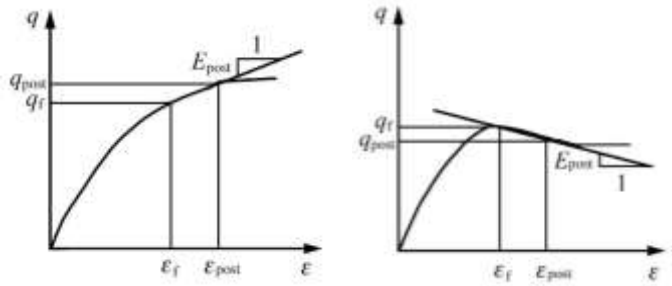

(a)Strain hardening (b)Strain softening

Fig. 8 The definition of post-failure modulus (Revised from [29])

In principle, determination of SSM's failure strain and strength should strictly comply with soil testing method standards while considering characteristics of stress and strain. In pattern I (strain hardening), ε_f typically ranges from 2% to 3%, corresponding to its associated stress q_f. Conversely, in pattern II (strain softening), q_f represents the peak stress, whereas ε_f represents corresponding strains. The actual post-failure value ε_{post} is obtained from observed strain-strain curves , indicating an approximate increase of 1% to 5% beyond failure strains, along with their respective strains denoted as q_{post}.

Additionally, the stress-strain relationship can be characterized by the sign of E_{post}, where a positive value indicates strain hardening and a negative value indicates strain softening (Fig.8). It is evident that E_{post} is dependent on the confining pressure σ_3 [28, 29].

$$E_{post} = f(\sigma_3) \#(10)$$

Based on the definition of post-failure modulus, the quantitative investigation of stress-strain relationship transition can be conducted by analyzing the variation of E_{post} with respect to σ_3. In particular, $E_{post} = 0$ represents the point of intersection between f (σ_3) and the horizontal

axis, which serves as a critical point indicating the transition in stress-strain relationship. The confining pressure σ_3 corresponding to $E_{post} = 0$ is considered as the critical confining pressure $\sigma_{3,cr}$ for this transition.

3.3 Application of Post-Failure Modulus E_{post} in Tests

To verify the validity of E_{post}, Table 2 provides the values of parameters ($\varepsilon_f, q_f, \varepsilon_{post}, q_{post}$) as defined in Eq. (9), Meanwhile, Fig.9 illustrated the various critical confining pressures derived from the experimental data presented in Fig.5. It is important to note that, given the dependency of these parameter values on the coordinates of the stress-strain curve depicted in Fig. 5, a certain degree of discrepancy may exist between the measured and tested values. Nevertheless, this deviation has negligible influence on the prediction of the overall stress-strain relationship trend.

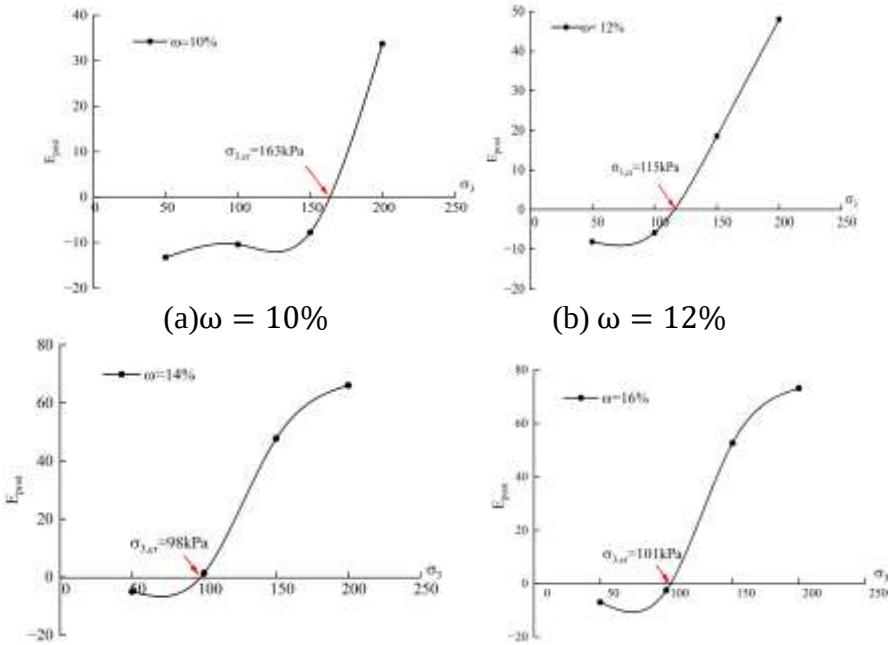

(a)ω = 10% (b) ω = 12%

(c)ω = 14% (d) ω = 16%

Fig. 9 The critical confining pressure under different moisture content for SSM

Table 2 The parameters values ($\varepsilon_f, q_f, \varepsilon_{post}, q_{post}$) of SSM samples

Water content/%	Confining pressure/kPa	ε_f/%	q_f/kPa	ε_{post}/ %	q_{post}/kPa	E_{post}	Strain type
10%	50	3.09	353	4.07	340	13.27	Softening
	100	3.95	535	4.62	528	10.45	Softening
	150	4.27	675	5.04	669	7.79	Softening
	200	3.22	770	4.11	800	33.71	Hardening
12%	50	2.82	331	3.68	324	-8.14	Softening
	100	4.99	537	5.85	532	-5.81	Softening
	150	2.75	540	3.29	550	18.52	Hardening
	200	2.74	730	3.49	766	48.00	Hardening
14%	50	2.82	298	4.01	292	-5.04	Softening
	100	2.12	379	3	418	44.32	Hardening
	150	2.01	514	3.12	567	47.75	Hardening
	200	3.25	612	4.43	690	66.10	Hardening
16%	50	6.53	300	7.25	295	-6.94	Softening
	100	7.11	424	8.34	416	-6.50	Softening
	150	4.29	450	5.62	520	52.63	Hardening

	200	4.46	610	5.28	670	73.17	Hardening

3.4 Application of CPM Model in Tests

As shown in Fig. 10, the stress-strain curve of SSM can be accurately represented by Eq. (1). The CPM model demonstrates high precision in capturing stress-strain curves with various degrees of hardening and softening. The coefficient of determination, R^2, consistently exceeds 0.9 for confining pressures of 50 kPa and 100 kPa, confirming the model's ability to precisely describe the stress-strain relationship, which is fully adequate for engineering applications. Additionally, it is evident that when $\sigma_3 < \sigma_{3,cr}$,, the curves predicted by the CPM model exhibit softening behavior; conversely, when $\sigma_3 > \sigma_{3,cr}$, they display hardening characteristics.

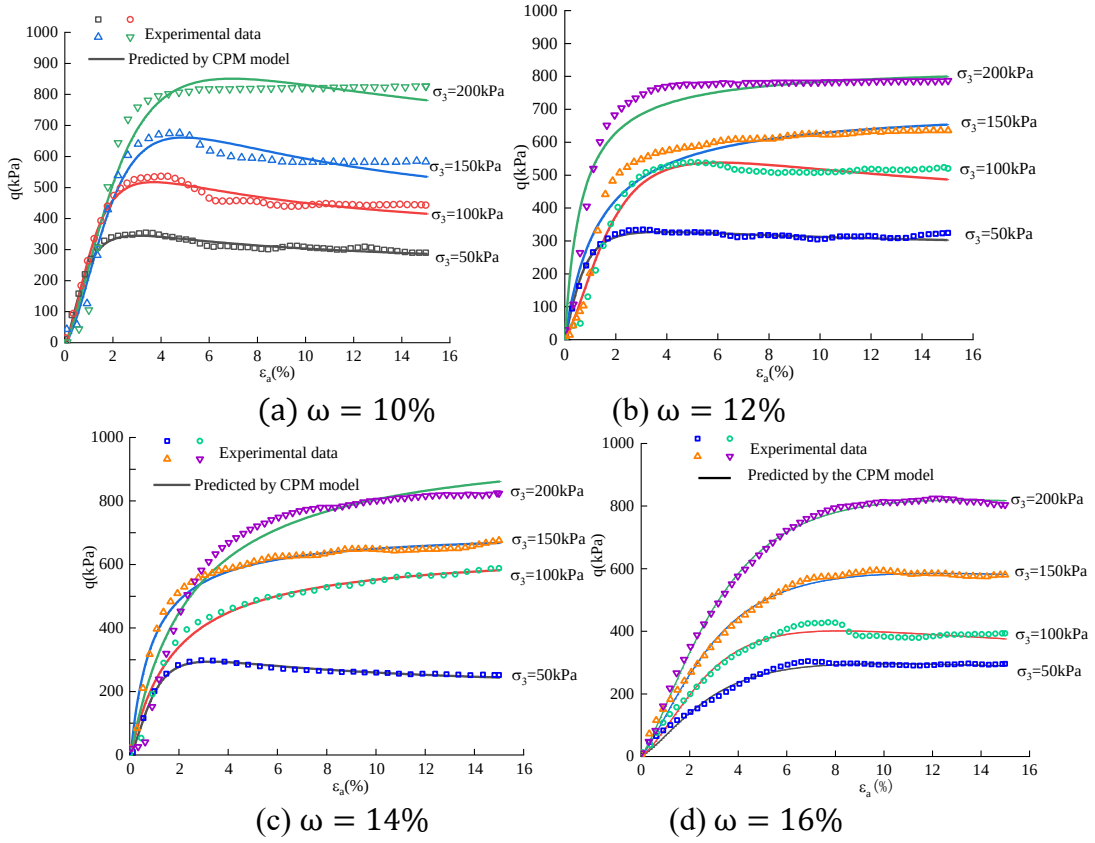

(a) ω = 10% (b) ω = 12%

(c) ω = 14% (d) ω = 16%

Fig.10 Stress-strain curves described by the CPM model

4. Model Verifications

The CPM model not only accurately characterizes the stress-strain behavior observed in the test, but also enables prediction of the critical confining pressure, which serves as a rough indicator for determining stress-strain classification. The validity of this model in describing stress-strain relationships has been verified through measured data from SSM experiments. To further demonstrate its broad applicability to other soils or materials, three cases were examined to validate the suitability of the CPM model and simultaneously predict the critical confining pressure.

4.1 Verification on Loess

The consolidated undrained triaxial tests on undisturbed loess samples were performed by Wang et al [23], with an initial dry density of $\rho_d = 1.36\mathrm{g}\cdot cm^{-3}$ and water content of $w = 13.0\%$. The test results reveal that the stress-strain relationship of the samples demostrate both softening and hardening characteristics. Subsequently, the CPM model was utilized to characterize the stress-strain behavior under various confining pressures (100, 200, 300, and 400kPa). This allowed for a comparison between the modeled data and experimental results, as well as the prediction of the critical confining pressure, as illustrated in Fig. 11. Notably, the coefficient of determination (R^2) exceeds 0.92 for all tested confining pressures (100, 200, 300, and 400 kPa),

indicating a strong correlation between the predicted and measured stress-strain curves. Additionally, based on the definition of post-failure modulus in the CPM model, a critical confining pressure of $\sigma_{3,cr}$ = 191 kPa (Fig. 12) was obtained, which aligns closely with the value $\sigma_{3,cr}$ = 217 kPa calculated using the linear interpolation method in the CPE model.

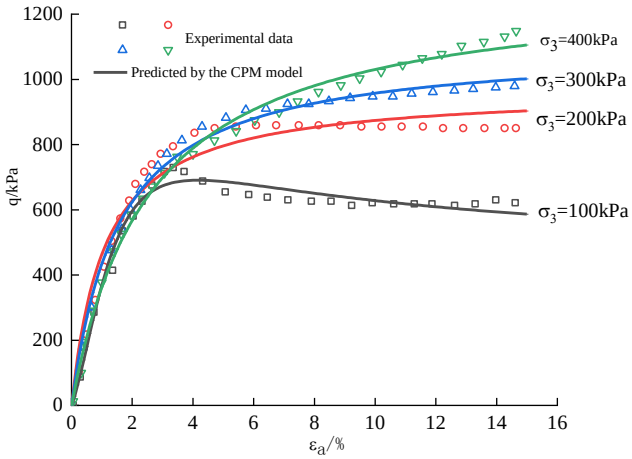

Fig. 11 Comparison between CPM model and experimental data in Loess

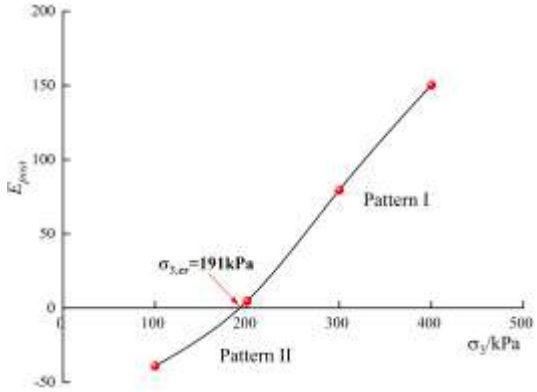

Fig. 12 $E_{post} - \sigma_3$ relation in Loess sample

4.2 Verification on Municipal Solid Waste Incineration Bottom Ash (MSWIBA)

The stress-strain behavior of MSWIBA was systematically investigated by Xiang et al. [29] through a series of standardized consolidated drained triaxial tests, considering various curing ages (ranging from 3 to 28 days) and confining pressures (spanning from 50 to 400 kPa). For instance, with a curing time of 28 days, Fig. 13 demonstrates the variation of deviatoric stress with axial strain in these tests, highlighting significant softening and hardening behaviors. Furthermore, Fig. 14 illustrates the stress-strain curves predicted by the CPM model. Notably, the CPM model exhibits excellent agreement with the experimental data and precisely captures the stress-strain relationship. A critical confining pressure of $\sigma_{3,cr}$= 133 kPa is identified , which surpasses classical models in terms of accuracy.

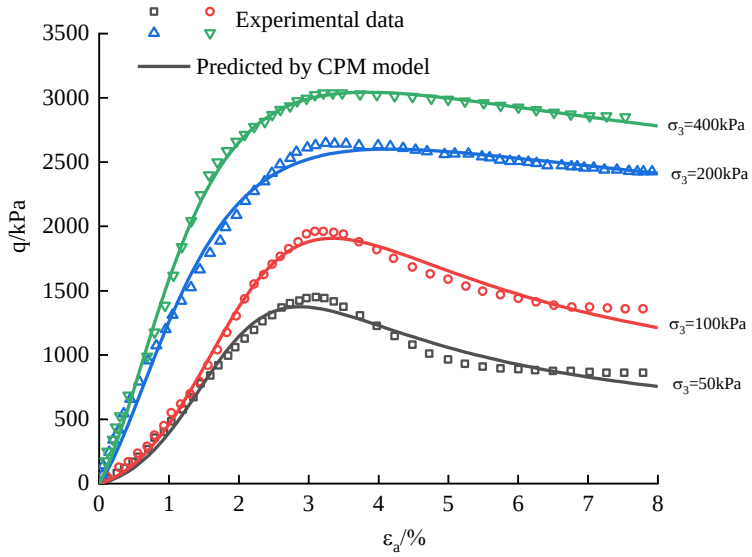

Fig. 13 Comparison between CPM model and experimental data in MSWIBA

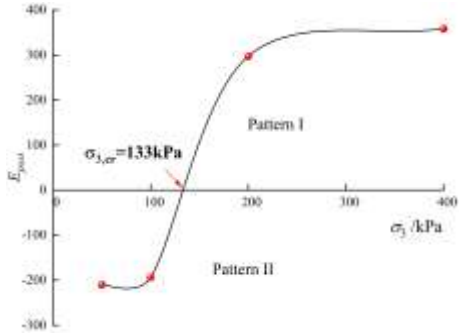

Fig. 14 $E_{post} - \sigma_3$ relation in MSWIBA (Curing time=28days)

4.3 Verification on Lime Reinforced Silt

To improve the mechanical properties of silt, a specified quantity of lime was introduced into the soil sample to enhance both soil strength and water stability in the mixture [30]. For instance, with a lime content of 5%, the stress-strain curves of lime-treated silt under various confining pressures closely resemble those illustrated in Fig. 5. When the lime content is set at 5%, under higher confining pressures (200 kPa and 300 kPa), the principal stress difference increases with axial strain; however, this increase progressively diminishes as axial strain continues to grow. The latter portion of the curve shows approximate flatness, indicating strain hardening behavior. In contrast, when incorporating 5% lime and applying lower confining pressures of 50 kPa and 100 kPa, a noticeable decrease occurs after reaching the peak values on the curves, demonstrating strain softening. Similarly, the CPM model was utilized to verify its applicability (see Fig. 15), from which a transition critical confining pressure $\sigma_{3,cr}$ = 113 kPa was derived (Fig. 16). Both results exhibit excellent agreement with the experimental data.

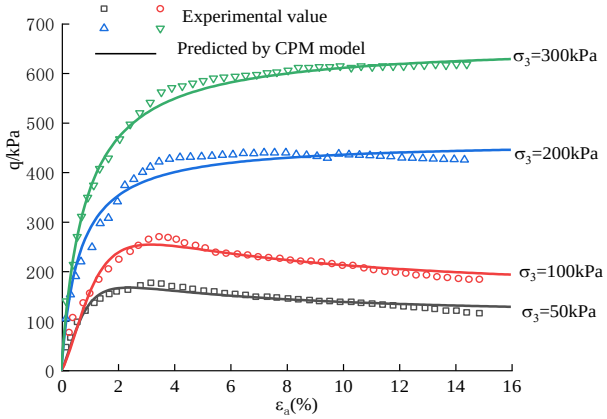

Fig. 15. Comparison between CPM model and experimental data in lime reinforced silt

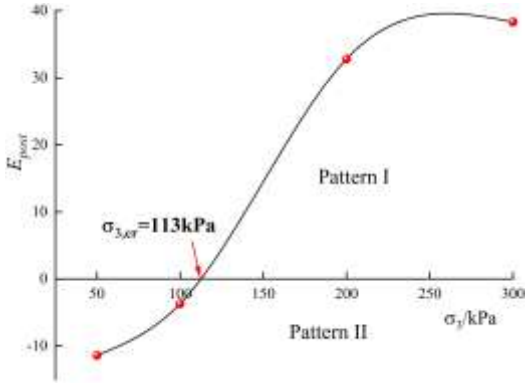

Fig. 16. $E_{post} - \sigma_3$ relation in lime reinforced silt (mixing ratio =5%)

5. Transition Mechanism

Under the same confining pressure, the stress-strain relationship of remolded SSM with varying initial water content does not align consistently with the development of axial strain. This transformation is primarily attributed to the inherent characteristics of silt, which consists of a high proportion of uniformly sized fine particles and lacks clay particles. Even when compaction achieves maximum dry density, the soil still contains numerous pores due to insufficient clay filling between the voids formed by the accumulation of fine particles [31]. These pores serve as storage spaces for water infiltration into the soil matrix. At low water content, the intergranular bonding force in SSM samples remains strong. However, as water content increases, some smaller particles detach and aggregate into larger particles due to weakened inter-particle bonding forces. This results in reduced mechanical interaction among larger particles, increased porosity, and diminished intergranular bonding force and internal friction angle [32]. Consequently, both the strength and elastic modulus of the samples decrease. As a result, specimens exhibit reduced resistance to deviatoric stress during shear tests, thereby influencing the shape of their stress-strain curve. Notably, under specific confining pressures, there exists a critical water content point that delineates the transition between stress softening and hardening behaviors.

Also, the stress-strain transition influenced by confining pressure can be described as follows. When the confining pressure is relatively low, the particles continue to undergo compression under axial loading, leading to a reduction in pore volume between the particles and a gradual increase in deviatoric stress within the sample. Once the deviatoric stress reaches its peak, the pore volume between the particles is minimized, and the particle matrix begins to fail. However, this failure process of the particle skeleton occurs gradually, resulting in a progressive decrease in deviatoric stress of the SSM sample with increasing strain. In other words, the stress-strain curve exhibits strain-softening behavior. During triaxial shear testing at relatively high confining pressures, the pores within the SSM samples are continuously compressed as the deviatoric stress gradually increases before reaching its peak value.

Once the pore volume is minimized to its maximum extent, particle skeleton fracture should occur; however, due to the high confining pressure acting on it, the axial bearing capacity of the particle skeleton increases, preventing its failure [33,34]. Consequently, partial stresses within the particle skeleton increase but do so slowly with increasing strain until they eventually stabilize, demonstrating strain-hardening behavior.

6. Conclusions

The stress-strain relationship of soil is fundamental to ensuring the accuracy and reliability of numerical calculations in geotechnical engineering. Accurately describing and predicting the stress-strain behavior of materials under diverse stress conditions is critically important. In this study, the CPM model is utilized to characterize and predict the stress-strain relationship of SSM under varying confining pressures with high precision. The primary conclusions are summarized as follows:

(1) By incorporating a transition factor, the CPM model is formulated to comprehensively describe both strain softening and hardening behaviors. This unified nonlinear equation integrates the Duncan-Chang model with the NHRI model, thereby providing a clear explanation of the mechanisms underlying softening and hardening phenomena.

(2) Through the introduction of the post-failure modulus, the CPM model not only characterizes the stress-strain relationship but also quantitatively determines the critical confining pressure. This parameter can be employed to identify the strain type under specific confining pressures and predict the stress-strain curve across a range of confining pressures.

(3) To enhance the applicability of the CPM model, test results and three additional practical cases are presented to validate its suitability for applications in dam decomposition, loess management, municipal solid waste incineration bottom ash (MSWIBA) treatment, and lime-reinforced silt soil. This provides a systematic and straightforward approach for preliminary strain prediction and aids in identifying stress-strain transitions.

(4) The transition mechanisms of stress-strain curves under varying water content and confining pressure can primarily be attributed to the inherent characteristics of silt as described in the SSM model and the hysteresis effect of soil skeleton deformation, respectively. A critical threshold of confining pressure and moisture content exists, which determines the transformation from strain softening to strain hardening.

Overall, this study enhances the understanding of stress-strain transitions in various types of soils and provides valuable insights for geotechnical engineering practices. Future research should concentrate on expanding the comprehension of stress-strain transitions under diverse operational conditions. This involves investigating the effects of temperature and loading rates on stress-strain relationships. Moreover, integrating advanced computational techniques to simulate stress-strain transitions could offer more profound insights. Additionally, the development of novel constitutive models capable of accurately predicting stress-strain transitions under complex loading scenarios is essential.

Credit authorship contribution statement

Ya Wang: Conceptualization, Methodology, Writing original draft; Hongyu Wang: Writing review& editing, Resource. Liucheng Chang; Numerical analysis, Validation.

Data Availability: Data will be made available on request.

Clinical Trial: Not Applicable

Consent to Publish Declaration: Not applicable

Ethics and Consent to Participate Declarations: Not applicable

Declaration of Competing Interest

Research grants from funding agencies Natural Science Foundation of China (Grant No.41962016) and the Natural Science Foundation of NingXia (2023AAC03387, 2023 AAC02023). The authors would like to acknowledge all these sources of financial support and express the sincerest gratitude. In addition, the authors declare that they have no known competing financial interest or personal relationships that could have appeared to influence the work reported in this paper.

Acknowledgements

The authors would like to thank the Natural

Science Foundation of China (Grant No.41962016) and the Natural Science Foundation of NingXia (2023AAC03387, 2023AAC02023). The authors would like to acknowledge all these sources of financial support and express the sincerest gratitude. In addition, the authors greatly appreciated the reviewers for their valuable comments and suggestions and the professionals for polishing the language for improving this paper.

References

1. Ran D, Luo Q, Zhou Z, Wang G, Zhang X. Sediment retention by check dams in the Hekouzhen-Longmen Section of the Yellow River. Int J Sediment Res. 2008;23(2):159-66.
2. Hou K, Qian H, Zhang Yuting, Zhang Qiying, Qu Wengang. New insights into loess formation on the southern margin of the Chinese Loess Plateau. CATENA,2021, Volume 204,105444.
3. Quiñonero-Rubio JM, Nadeu E, Boix-Fayos C, De Vente J. Evaluation of the effectiveness of forest restoration and check-dams to reduce catchment sediment yield. Land Degrad Dev. 2016;27(4):1018-31.
4. Zhao, J., Luo, X., Ma, Y., Shao, T., and Yue, Y., Soil characteristics and new formation model of loess on the Chinese Loess Plateau. 2017, Geosciences
5. Samad, N., Chauhdry, M. H., Ashraf, M., Saleem, M., Hamid, Q., Babar, U., Tariq, H., and Farid, M. S., Sediment yield assessment and identification of check dam sites for Rawal Dam catchment: Arabian Journal of Geosciences. 2016.
6. Dong H, Song Y, Chen L, Liu H, Fu X, Xie M. Soil erosion and human activities over the last 60 years revealed by magnetism, particle size and minerals of check dams sediments on the Chinese Loess Plateau. Environmental earth sciences. 2022;81(5):1-15.
7. Wang, Y; Wang, HY and Guo, LP, Microstructural Analysis on Shear Behavior of New-fill and Silt Interface in Check Dam. Journal of soils and sediment,2024:24 (9) , pp.3223-3237
8. Chang, LC; Wang, Y and Wang, HY. Influence of sand content on mechanical properties of sand-silt mixtures from check dam deposits in the Loess Hilly of Ningxia, China. Plos one. 2023; 18 (11)
9. Pongpipat, A., Phimmawat, I., and Victor, N. K., Three-dimensional stress–strain and strength behavior of silt–clay transition soils. Canadian Geotechnical Journal. 2023.
10. Monkul MM, Ozden G. Compressional behavior of clayey sand and transition fines content. Eng Geol. 2007;89(3-4):195-205.
11. Xenaki VC, Athanasopoulos GA. Liquefaction resistance of sand–silt mixtures: an experimental investigation of the effect of fines. Soil Dyn Earthq Eng. 2003;23(3):1-12.
12. Sadrekarimi A. Influence of fines content on liquefied strength of silty sands. Soil Dyn Earthq Eng. 2013; 55:108-19.
13. Duncan, J M, and Chang, C Y, Nonlinear analysis of stress and strain in soils. Journal of the Soil Mechanics and Foundations Division, ASCE, 1970,96(5), 1629-1653.
14. Wang, W., Song, X.J., Ling, H., Lu, T.H., Zhou, G.W. Composite exponential-hyperbolic model for stress-strain curve of seashore soft soil. China Journal of Geotechnical. Engineering. 2010 b,32(9):1455-1459.
15. Wang L Q, Lu Z G and Shao S J, Composite power-exponential nonlinear model of rock and soil mass. Chinese Journal of Rock Mechanics and Engineering, 2017,36(5), 10.
16. Wang W, Ling H, Xu S D, et al. Composite Tangent-Exponent Model for Skeleton Stress-Strain Curve of Soft Soil under Dynamic Loading. Advanced Materials Research, 2010, 108-111:1092-1096.
17. Yin D.S., Ren J.J., He C.L. Stress-stain relation of soft soil based on fractional calculus operators theory. Chinese Journal of Rock Mechanics and Engineering, 2009,28 (Supp.1)：2973-2979.
18. Sheng Z J. A nonlinear dilatant stress-strain model for soils and rock materials. Hydro-Science and engineering,1986.4:3-16.
19. Al-Shayea, N., Abduljauwad, S., Bashir, R., Al-Ghamedy, H., and Asi, I. Determination of parameters for a hyperbolic model of soils. Geotechnical Engineering, 2003,156(GE2), 105-117.
20. Liu X, Liu J, Tian Y, Chang D, Hu T. Influence of the freeze-thaw effect on the Duncan Chang model parameter for lean clay. Transp Geotech. 2019(21):1-9.

21. Jia P, Khoshghalb A, Chen C, Zhao W, Dong M, Esgandani GA. Modified Duncan-Chang constitutive model for modeling supported excavations in granular soils. International journal of geomechanics. 2020;20(11):1-13.
22. Wang Y Q, Xin. H. B., Stable deformation characteristics of Dashihe tailing, Journal of Hydraulic Engineering, 1995, 11:56-62.
23. Wang L, Li K, Wang Z, Description and prediction of stress-strain curve of loess. Engineering Geology, 2022.
24. Huang B, Xu R Q, Wang J C, Soil stress-strain relationship transition curve and parameter study. Cryogenic architectural technology, 2006(1):3.
25. Y Wu, N Li XZ Wang, Cui et al., Experimental investigation on mechanical behavior and particle crushing of calcareous sand retrieved from South China Sea. Engineering Geology,2021 (280),105932
26. Wu Y, Cui J, Huang et al. Correlation of Critical State Strength Properties with Particle Shape and Surface Fractal Dimension of Clinker Ash, International Journal of Geomechanics, 2021:(21) 6
27. ASTM. 2006.Standard practice for classification of soils for engineering purposes (unified soil classification system). ASTM D2487-11. West Conshohocken, PA: ASTM.
28. Wang CH, Li GX. 2001. Analysis of problem of pattern transition in stress-strain relations of soils. Rock & Soil Mechanics. 25(8):1185–1190. in Chinese)
29. Xiang G. S, Song D.Q. and Zhuo C. Investigated stress-strain relationships of municipal solid waste incineration bottom ash, Natural Hazards and Risk,2020,11:1, 2431-2448
30. Hao J.B., Wei X.M., Yao J., et al. Strength characteristics and microstructure analysis of wheat straw reinforced soil. Journal of Tongji University (Natural Science), 2018, 47(06).
31. Gitau A N, Gumbe L O, Biamah E K. Influence of soil water on stress-strain behavior of a compacting soil in semi-arid Kenya. Soil & Tillage Research, 2006, 89(2): 144-154.
32. Maziyar A, Erfan C, and Mohammad M, Behavior of unsaturated sand-silt mixture through equivalent intergranular void ratio concept. Journal of Geoengineering, 2020: 15 (3):109-121.
33. Pongpipat A, Jerry A. Y., Victor N. K, Stress-Strain and Strength Characteristics of Silt-Clay Transition Soils, Journal of Geotechnical and Geoenvironmental Engineering, 2012,138(10)
34. Li Q, Xu X, Hu J, et al. Investigation of unsaturated frozen soil behavior: Phase transformation state, post-peak strength, and dilatancy. Soils and foundations, 2018, 58(4): 928-940.